atmosphere

MDPI

Article

Trends and Spatiotemporal Patterns of the Meteorological Drought in the Ili River Valley from 1961 to 2023: An SPEI-Based Study

Su Hang [1], Alim Abbas [2], Bilal Imin [1,3,*], Nijat Kasim [1,3] and Zinhar Zunun [1,3]

[1] College of Resources and Environment, Yili Normal University, Yili 835000, China; 220801080@ylnu.edu.cn (S.H.); nejatkasim@126.com (N.K.); 20063@ylnu.edu.cn (Z.Z.)
[2] College of Resources and Environment, Xinjiang Agriculture University, Urumqi 830052, China; alimabbas@xjau.edu.cn
[3] Institute of Ecology and Environment, Yili Normal University, Yili 835000, China
* Correspondence: bilali@ylnu.edu.cn; Tel.: +86-183-9966-0357

Abstract: Drought presents significant challenges in arid regions, influencing local climate and environmental dynamics. While the large-scale climatic phenomena in Xinjiang, northwest China, are well-documented, the finer-scale climatic variability in subregions such as the Ili River Valley (IRV) remains insufficiently studied. This knowledge gap impedes effective regional planning and environmental management in this ecologically sensitive area. In this study, we analyze the spatiotemporal evolution of drought in the IRV from 1961 to 2023, using data from ten meteorological stations. The SPEI drought index, along with Sen's trend analysis, the Mann–Kendall test, the cumulative departure method, and wavelet analysis, were employed to assess drought patterns. Results show a significant drying trend in the IRV, starting in 1995, with frequent drought events from 2018 onwards, and no notable transition year observed from wet to dry conditions. The overall drought rate was −0.09 per decade, indicating milder drought severity in the IRV compared to broader Xinjiang. Seasonally, the IRV experiences drier summers and wetter winters compared to regional averages, with negligible changes in autumn and milder drought conditions in spring. Abrupt changes in the drying seasons occurred later in the IRV than in Xinjiang, with delays of 21 years for summer, and over 17 and 35 years for spring and autumn, respectively, indicating a lagged response. Spatially, the western plains are more prone to aridification than the central and eastern mountainous regions. The study also reveals significant differences in drought cycles, which are longer than those in Xinjiang, with distinct wet–dry phases observed across multiple time scales and seasons, emphasizing the complexity of drought variability in the IRV. In conclusion, the valley exhibits unique drought characteristics, including milder intensity, pronounced seasonal variation, spatial heterogeneity, and notable resilience to climate change. These findings underscore the need for region-specific drought management strategies, as broader approaches may not be effective at the subregional scale.

Keywords: Ili River Valley; climate change; meteorological drought; spatiotemporal evolution

check for updates

Academic Editors: Seontae Kim and Anthony R. Lupo

Received: 31 October 2024
Revised: 22 December 2024
Accepted: 27 December 2024
Published: 2 January 2025

Citation: Hang, S.; Abbas, A.; Imin, B.; Kasim, N.; Zunun, Z. Trends and Spatiotemporal Patterns of the Meteorological Drought in the Ili River Valley from 1961 to 2023: An SPEI-Based Study. *Atmosphere* **2025**, *16*, 43. https://doi.org/10.3390/atmos16010043

Copyright: © 2025 by the authors. Licensee MDPI, Basel, Switzerland. This article is an open access article distributed under the terms and conditions of the Creative Commons Attribution (CC BY) license (https://creativecommons.org/licenses/by/4.0/).

1. Introduction

Climate extremes, including droughts, have become critical global challenges due to the intensification of global warming [1,2]. The sixth Intergovernmental Panel on Climate Change (IPCC) report highlights that the global annual average surface temperature has

risen by 1.09 °C over the past century [3,4]. These temperature changes are reflected in the increasing frequency of extreme climate events, particularly severe droughts [5]. Droughts are among the most devastating natural disasters worldwide, causing substantial economic and social disruption [6,7]. They are characterized by prolonged periods of abnormally low precipitation and high evapotranspiration, and are especially destructive in terms of water resources, agricultural productivity, and ecological stability [8–14]. Furthermore, meteorological droughts significantly affect vegetation productivity, influencing terrestrial carbon storage and the global carbon cycle [15–17]. Thus, droughts exacerbated by global warming have become one of the most pressing concerns worldwide.

Arid and semi-arid regions, with their unique geographical locations and fragile ecological environments, face unprecedented challenges due to rising temperatures [18,19]. The spatiotemporal patterns of drought are complex and vary across different regions. While some semi-arid and arid areas experience more frequent droughts, others may face increased precipitation or fluctuating drought patterns [20,21]. These patterns are influenced by regional climate variability, atmospheric circulation, and oceanic conditions, such as the El Niño–Southern Oscillation (ENSO) [22]. Previous studies have documented significant regional variations in drought patterns. For example, precipitation has increased in southern Asia, southern Africa, and the northeastern drylands of North America, while severe droughts have been observed in central North America, southwestern South America, eastern Africa, and western Asia [23–26]. China, particularly its northwestern regions, has experienced considerable drought-related challenges, necessitating comprehensive scientific investigation [27,28]. Recent studies have focused on understanding the trends, causes, and effects of drought in this region to inform better management and mitigation strategies [29–31]. While these studies contribute to a broader understanding of drought dynamics, most focus on large-scale regions, often overlooking localized areas with distinct geographical and topographical features. To address this gap, detailed analyses are required to explore the spatiotemporal variability in drought incidence in these subregions.

The Ili River Valley, located in the semi-arid region of northwestern China within the Xinjiang Uygur Autonomous Region, is a vital agricultural and pastoral base [27,32]. The valley features a unique vertical natural zonation, rich vegetation resources, and serves as a critical ecological barrier [33,34]. Designated as one of China's five Key Terrestrial Biodiversity Areas, it is increasingly vulnerable to ecosystem degradation driven by climate change [35,36]. This ecological fragility necessitates urgent interventions to preserve its valuable resources. While previous studies have aimed to understand the climatic characteristics of the Ili River Valley, most have relied on individual case analyses or mean values averaged over extended periods, resulting in a lack of a comprehensive understanding of the region's drought characteristics.

This study aims to address this gap by (1) quantifying drought severity in the Ili River Valley using the Standardized Precipitation Evapotranspiration Index (SPEI) to objectively assess meteorological drought conditions; (2) analyzing spatial and temporal trends, along with long-term drought characteristics in the Ili River Valley from 1961 to 2023, utilizing Sean's trend analysis, the Mann–Kendall test, and the cumulative anomaly method; (3) employing wavelet analysis to visually depict the periodicity and long-term patterns of drought in the region.

2. Materials and Methods

2.1. Trial Area

The Ili River Valley (specifically referring to the upper reaches of the Ili River, China) is located within the temperate continental semi-arid climate zone (42°14′16″~44°53′30″; 80°09′42″~84°56′50″). The region features a western-facing, trumpet-shaped topography,

with the north, east, and south sides bordered by the Tianshan Mountains (Figure 1). This unique terrain allows for annual moisture influx from the Atlantic Ocean, resulting in a warm and humid climate distinct from the more arid and semi-arid regions of Xinjiang. The mean annual temperature is 10.4 °C, with total annual precipitation averaging 417.6 mm, reaching up to 1000 mm in high-altitude areas [35]. Due to these conditions, the region is often referred to as the "Independent Wet Island" and is recognized as the area with the highest precipitation in Xinjiang. Additionally, the mountains to the north and south block hot, dry airflows from the Gurbantunggut and Taklamakan Deserts, as well as cold, dry airflows from Siberia [35]. Abundant precipitation and seasonal melting from the western Tianshan Mountains play a significant role in water circulation and ecological stability within the region. Rich in water resources, the area also supports high biodiversity and well-developed agriculture [37], serving as a critical ecological buffer in northwest China [35].

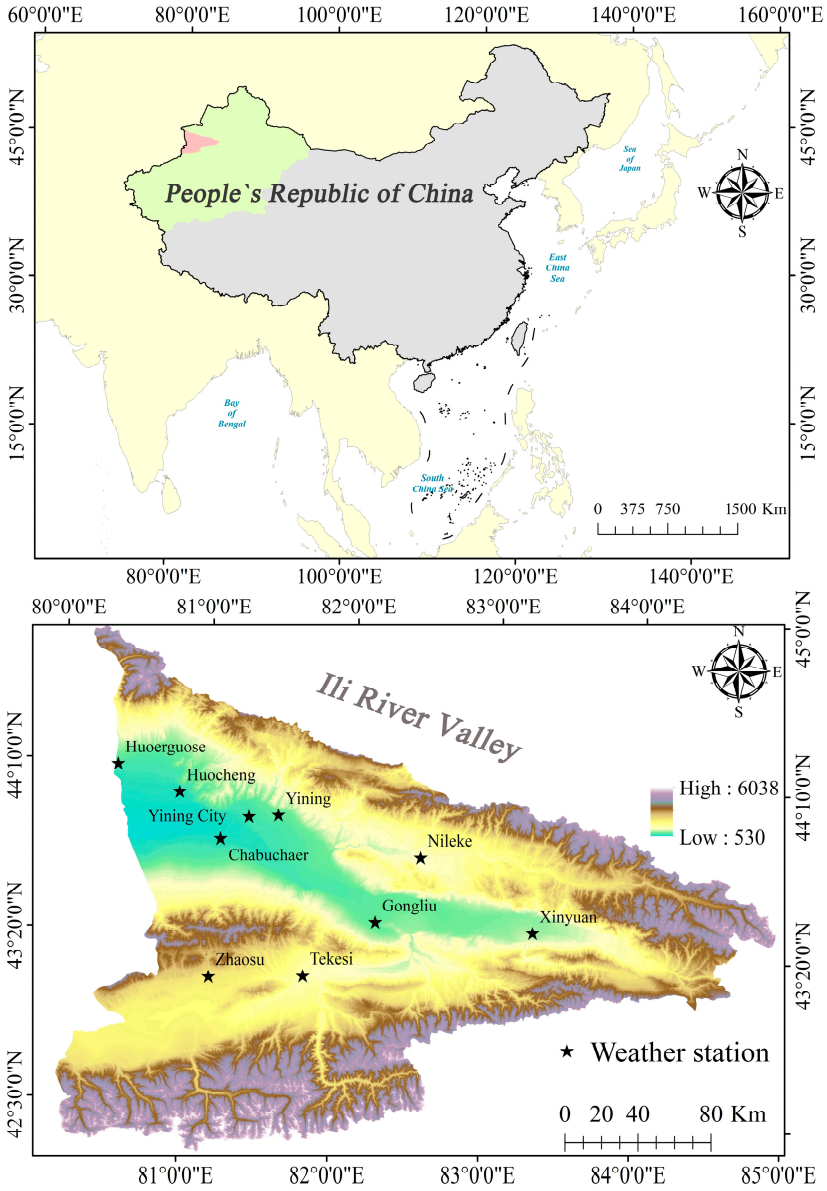


Figure 1. Sketch map of the study area (the black line represents the country border, the green area indicates the Xinjiang Uyghur Autonomous Region of China, and the red area denotes the Ili River Valley).

2.2. Data Acquisition and Processing

To characterize the fundamental climatic patterns of the Ili River Valley and calculate the Standardized Precipitation Evapotranspiration Index (SPEI), this study utilized meteorological data obtained from the China Meteorological Data Service Center (https://data.cma.cn/en, accessed on 5 February 2024). Data were collected from ten representative meteorological stations, as shown in Figure 1. These stations are spatially distributed to adequately represent the key meteorological conditions across the Ili River Valley. The meteorological parameters include daily maximum and minimum temperatures, precipitation, relative humidity, wind speed, and sunshine duration, with data organized by month and season. Seasons are defined as follows: spring (March to May), summer (June to August), autumn (September to November), and winter (December of the current year and January to February of the following year). All data underwent rigorous quality control procedures, including the removal of physically impossible values, statistical outlier detection using the standard deviation method, and temporal interpolation for missing values.

2.2.1. Standardized Precipitation Evapotranspiration Index (SPEI)

The SPEI, proposed by Vicente-Serrano et al. [38], integrates the advantages of the Palmer Drought Severity Index (PDSI) and the Standardized Precipitation Index (SPI) by incorporating potential evapotranspiration. This makes the SPEI particularly suitable for studying drought under global warming conditions and has led to its widespread adoption for calculating drought indices globally. The calculation steps for SPEI are as follows:

(1) Calculation of the hydrothermal balance:

$$D_i = P_i - (PET_i) \tag{1}$$

where D_i is the cumulative value of the difference between precipitation P_i and potential evapotranspiration PET_i in the calculated time scale; in this study, the Penman–Monteith model [39] was used to calculate the regional potential evapotranspiration rate. Equation:

$$PET = \frac{0.408\Delta(R_n - G) + \gamma(900/T + 273)U_2(e_a - e_d)}{\Delta + \gamma(1 + 0.34U_2)} \tag{2}$$

where R_n is net radiation at the surface (MJ/(m^2·d), estimated using sunshine duration data and the Angström formula; G is soil heat flux density (MJ/(m^2 d)), estimated as a fraction of net radiation based on FAO-56 guidelines; γ is psychrometric constant (kPa/°C), calculated based on atmospheric pressure; T is mean temperature (°C); U_2 is wind speed at 2 m altitude (m/s); Δ is a slope vapor pressure curve (kPa/°C), calculated using mean air temperature following the FAO-56 methodology; e_a is saturated water vapor pressure (kPa), computed using maximum and minimum temperatures; e_d is actual water vapor pressure (kPa), derived from relative humidity measurements.

(2) Constructing cumulative sequences of water surplus and deficit at different time scales:

$$\begin{cases} D_{i,j}^k = \sum_{i=13-k+j}^{j} D_{i,j} + \sum_{l=1}^{j} D_{i,l} & j < k \\ D_{i,j}^k = \sum_{i=j-k+1}^{j} D_{i,j} & j \geq k \end{cases} \tag{3}$$

where $D_{i,j}^k$ is the difference in cumulative precipitation evapotranspiration in k months from the j month of the i year.

(3) Normalize fitting the D_i data series. There may be negative values in the original data sequence D_i; therefore, the log-logistic probability distribution with three parameters is adopted:

$$f(x) = \frac{\beta}{\alpha}\left(\frac{x-\gamma}{\alpha}\right)^{\beta-1}\left[1+\left(\frac{x-\gamma}{\alpha}\right)^{\beta}\right]^{-2} \quad (4)$$

where f(x) is a probability density function, α, β and γ are scale parameters, shape parameters and origin parameters, respectively. The above parameters can be obtained by the linear moment method. On this basis, the cumulative probability under a given time scale can be obtained according to the following formula:

$$F(x) = \left[1+\left(\frac{\alpha}{x-\gamma}\right)^{\beta}\right]^{-1} \quad (5)$$

(4) Normalization of cumulative probability density:

$$P = 1 - F(x) \quad (6)$$

when the cumulative probability $P \leq 0.5$: $\omega = \sqrt{-2\ln(p)}$

$$SPEI = \omega - \frac{c_0 + c_1\omega + c_2\omega^2}{1 + d_1\omega + d_2\omega^2 + d_3\omega^3} \quad (7)$$

where $c_0 = 2.515517$, $c_1 = 0.802853$, $c_2 = 0.010328$, $d_1 = 1.432788$, $d_2 = 0.189269$, $d_3 = 0.001308$.

When the cumulative probability $p > 0.5$, P is represented by $1 - P$:

$$SPEI = -\left(\omega - \frac{c_0 + c_1\omega + c_2\omega^2}{1 + d_1\omega + d_2\omega^2 + d_3\omega^3}\right) \quad (8)$$

SPEI is a standardized drought index with multiple time scales, and the corresponding drought grade division refers to the standard table of SPEI drought grade division (Table 1). In this paper, SPEI1, SPEI3, and SPEI12 were used to analyze the variation in drought trend with time in the Ili River Valley. Based on the meteorological drought grade standard (GB/T20481-2017) implemented by the country in 2017, this paper formulates the SPEI drought grade classification standard suitable for the study area in Table 1.

Table 1. SPEI drought classification standard table [40].

Grade	Classification	SPEI Threshold
1	No drought	$-0.5 < SPEI$
2	Mild drought	$-1.0 < SPEI \leq -0.5$
3	Moderate drought	$-1.5 < SPEI \leq -1.0$
4	Severe drought	$-2.0 < SPEI \leq -1.5$
5	Extreme drought	$SPEI \leq -2.0$

2.2.2. Sen Trend Analysis and Mann–Kendall Test

The Theil–Sen median slope estimation method is a robust non-parametric statistical approach commonly used for trend analysis. This method calculates the median slope from all possible pairs of data points, effectively reducing the impact of outliers and anomalous observations. The non-parametric Mann–Kendall (MK) test and the Trend-Free Pre-Whitening Mann–Kendall (TFPW-MK) test is widely applied to assess the statistical significance of trends in time series data. In this study, we employed the non-parametric Mann–Kendall (MK) test for the following reasons: (1) to evaluate trends in long-term SPEI time series data; and (2) to ensure consistency with previous regional studies [21,28,31,40].

Unlike parametric methods, the non-parametric MK test does not require the assumption of a normal distribution and is resilient to missing values and outliers, making it particularly suitable for analyzing long-term climatic trends. To further validate our results, we also applied the TFPW-MK test, which yielded results consistent with the non-parametric MK test, thereby confirming the robustness of our analysis.

(1) Theil–Sen median slope estimation

In the present study, the Sen trend slope is employed to quantify the changing trend in the time series. The calculation formula for the Sen trend slope is as follows:

$$\beta = \text{Median}\left(\frac{SPEI_j - SPEI_i}{j - i}\right), \forall j > i \tag{9}$$

where $1 < j < i < n$; median is a median function; β is the trend of Sen, used to represent the ascending and descending degree of $SPEI_i$ trend. When $\beta > 0$, the $SPEI_i$ shows an upward trend, with larger values of β indicating a more pronounced increase, signifying intensifying drought conditions. Conversely, when $\beta < 0$, the $SPEI_i$ exhibits a downward trend, with smaller values of β indicating a more pronounced decrease, suggesting improving moisture conditions.

(2) Mann–Kendall trend test

Define a time series $SPEI_i$ ($i = 1, 2\ldots, n$) of the statistic S:

$$S = \sum_{i=1}^{n-1} \sum_{j=i+1}^{n} \text{sgn}\left(SPEI_j - SPEI_i\right) \tag{10}$$

Among them,

$$\text{sgn}\left(SPEI_j - SPEI_i\right) = \begin{cases} 1 SPEI_j - SPEI_i > 0 \\ 0 SPEI_j - SPEI_i = 0 \\ -1 SPEI_j - SPEI_i < 0 \end{cases} \tag{11}$$

The constructed statistic sequence S_i = ($i = 1, 2\ldots, n$) approximately follows a normal distribution with mean E(S) = 0 and variance

$$\text{Var}(S) = \frac{n(n-1)(2n+5)}{18} \tag{12}$$

when $n \geq 10$, the standard normal test statistic Z for S can be calculated by the following formula:

$$Z \begin{cases} \frac{S-1}{\sqrt{\text{Var}(S)}} & S > 0 \\ 0 & S = 0 \\ \frac{S+1}{\sqrt{\text{Var}(S)}} & S < 0 \end{cases} \tag{13}$$

At a given confidence level α, if $|Z| \geq Z_ (1 - \alpha/2))$, rejecting the null hypothesis that time series $\{SPEI_i\}$ is trendless. It indicates that $\{SPEI_i\}$ has a significant upward ($Z > 0$) or downward ($Z < 0$) trend.

(3) MK abrupt test

Construct time series $SPEI_i$ ($i = 1, 2\ldots, n$) of the order column S_k:

$$S_k = \sum_{i=1}^{k} r_i (k = 1, 2, \ldots, n) \tag{14}$$

Among them,

$$r_i = \begin{cases} 1, x_i > x_j \\ 0, x_i < x_j \end{cases} \quad j = 1, 2, \ldots, i; i = 1, 2, \ldots, n \tag{15}$$

Statistic UF_k is defined assuming that the time series is random and independent:

$$UF_k = \frac{S_k - E_{S_k}}{\sqrt{Var(S_k)}} \tag{16}$$

Among them, E_{Sk} and Var (S_k) is the mean and variance of S_k, calculated as follows:

$$E_{S_k} = \frac{k * (k-1)}{4} \tag{17}$$

$$Var(S_k) = \frac{k * (k-1) * (2k+5)}{72} \tag{18}$$

where UF_k is the standard normal distribution, given the significance level α, find the normal distribution table, if it indicates that there is a significant trend change in the sequence. The original time series is arranged in reverse order, the above process is repeated. At the same time, $UB_k = -UF_k$ is used to draw the two curves respectively. When the intersection point of the two curves is located within the critical line, the sequence can be considered to have a mutation, and the corresponding moment of the intersection point is the mutation start time.

2.2.3. Cumulative Anomaly Method

The cumulative anomaly method is a statistical technique employed to examine the trending patterns in time series data. This method involves calculating the difference between each value and its average value (i.e., anomaly) within the time series, followed by the accumulation of these anomaly values to form a new cumulative anomaly series. In this study, the cumulative anomaly method was utilized to analyze the long-term trends and periodic changes in SPEI data, thereby providing an effective means for understanding complex time series data. The calculation formula as follows:

$$CA = \sum (A(t) - u) \tag{19}$$

where CA is the cumulative anomaly; A(t) represents the value of the time series data at time t; u denotes the average value of the time series data; n is the total number of observations in the time series.

2.2.4. Wavelet Analysis

Wavelet analysis has been widely used for localized time-frequency analysis of signal characteristics. By examining the variations in signals in the time–frequency domain, this technique can highlight specific features and offers multi-resolution capabilities in both time and frequency spaces. It is particularly effective in identifying the evolving cycles and trends in non-stationary time series associated with climatic phenomena such as precipitation and temperature across various temporal scales. Wavelet analysis provides both qualitative and quantitative insights into the potential developmental trajectories of these phenomena.

In this study, MATLAB R2018a software was used for the wavelet analysis. Boundary effects were initially addressed using zero-padding and edge tapering techniques. The wavelet coefficients were then computed using the Morlet complex wavelet [41]. Contour visualizations of the relevant data were generated using Origin 2024 software.

3. Results

3.1. Analysis of Drought Dynamics in the Ili River Valley

Figure 2 illustrates the variations in drought conditions as identified by the Standardized Precipitation Evapotranspiration Index (SPEI) at different time scales in the study area from 1961 to 2023. SPEI-1 reflects short-term meteorological drought conditions, SPEI-3 captures seasonal meteorological drought variations, and SPEI-12 represents interannual meteorological drought patterns. As shown in the figure, both SPEI-1 (Figure 2a) and SPEI-3 (Figure 2b) exhibit high-frequency, large-amplitude fluctuations, clearly indicating subtle changes in SPEI values. In contrast, at the annual scale, the fluctuations in the SPEI-12 (Figure 2c) graph are more subdued, providing a clearer representation of long-term drought trends.

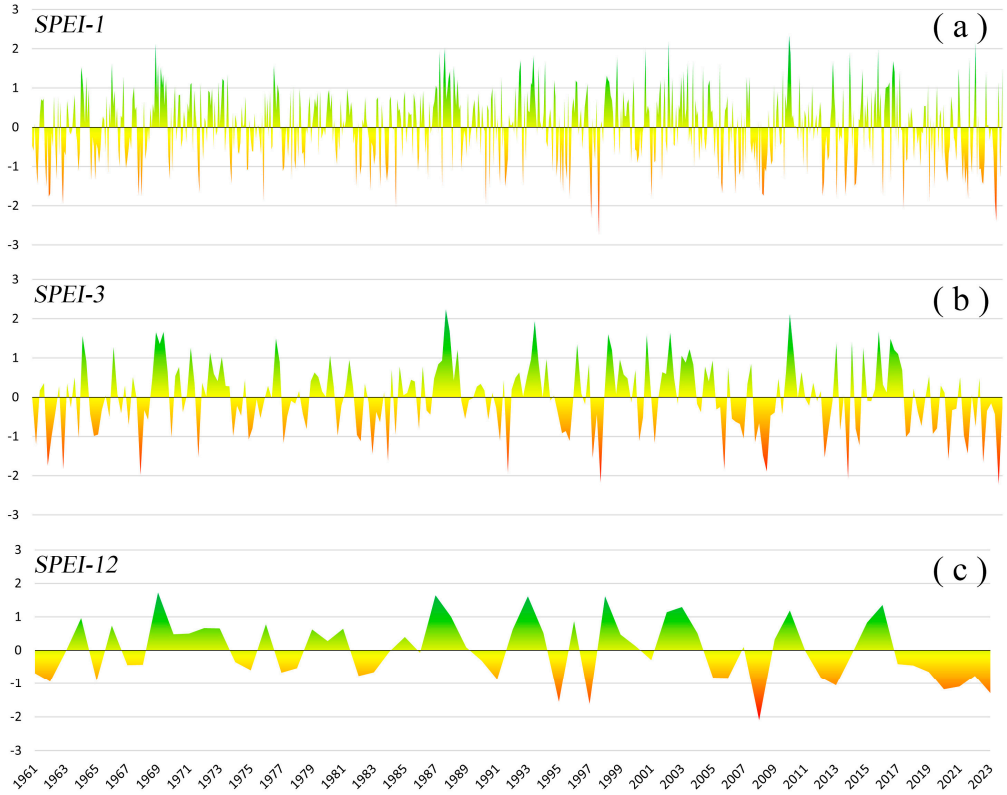


Figure 2. Fluctuation diagrams of SPEI-1 (**a**), SPEI-3 (**b**), and SPEI-12 (**c**) for the Ili River Valley region from 1961 to 2023 (The deeper the green, the more humid it is; the deeper the red, the more arid it becomes).

The research results indicate that, during the study period, the frequency and intensity of droughts in the Ili River Valley have significantly increased, with drought events occurring at varying degrees across all time scales. The analysis shows that short-term drought events exhibit higher frequency and intensity, while interannual drought patterns serve as critical indicators of long-term drought conditions. Examination of the SPEI-12 values reveals that significant drought conditions emerged after 1995, with particularly severe episodes occurring in 2008 (SPEI = −2.09), marking an extreme drought event in the Ili River Basin. Furthermore, consecutive observations from 2018 to 2023 confirm the region's persistent vulnerability to droughts of varying magnitudes.

3.2. Interannual Variations in the SPEI in the Ili River Valley

The interannual variation in SPEI in the Ili River Valley from 1961 to 2023, shown in Figure 3a, reveals a complex climatic trajectory. The SPEI values initially increase, followed

by a decline, with a peak of 1.73 in 1969, marking the wettest year, and a nadir of −2.09 in 2008, representing the driest year. A comprehensive 63-year analysis reveals a subtle but persistent downward trend in SPEI values. The Mann–Kendall (M-K) statistical test identified no statistically significant inflection point, suggesting no clear transition between wet and dry climatic regimes.

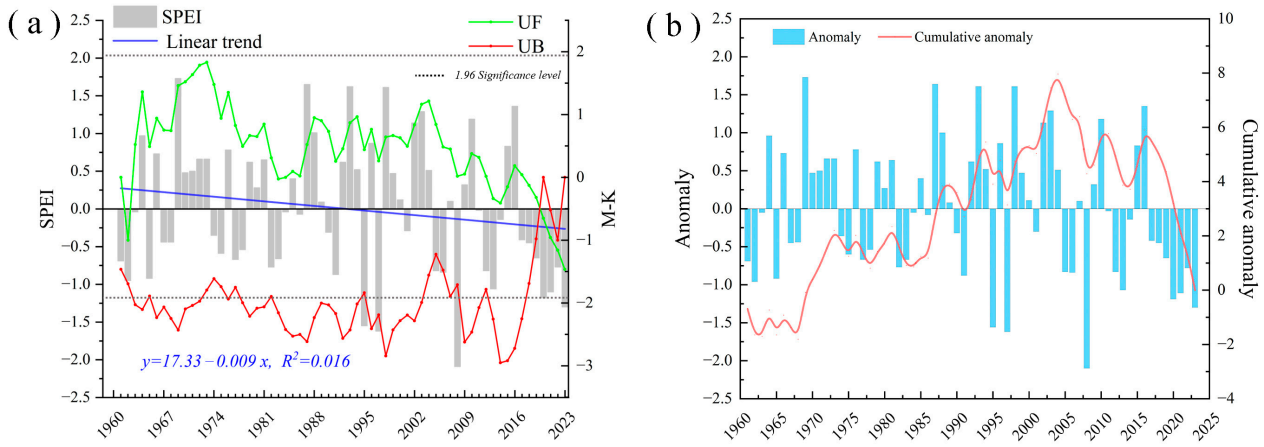


Figure 3. Results of the Mann–Kendall (M-K) mutation test (**a**) and anomaly analysis (**b**).

The anomaly and cumulative anomaly analyses provide an intuitive assessment of SPEI variations in the Ili River Valley from 1961 to 2023, as shown in Figure 3b. Over this period, the cumulative anomaly of the average annual SPEI displayed an initial increase followed by a decrease, forming an approximate "inverted V" shape. From 1961 to 2004, SPEI anomalies were predominantly positive, indicating a relatively humid period, with 1969 being the wettest year. In contrast, from 2005 to 2023, SPEI anomalies were mainly negative, signifying a more arid period. Notably, the SPEI anomaly values in 2008, 2013, 2020, 2021, and 2023 were all below −1, with 2008 reaching the lowest value of −2.1, marking a rapid intensification in drought severity since 2005. These findings suggest that drought conditions in the Ili River Valley have intensified in recent years, warranting further investigation and attention.

Figure 4 illustrates the spatial distribution of the SPEI slope in the Ili River Valley. The figure indicates that the drought trend across the entire Ili River Valley is intensifying, with all regions exhibiting negative Sen slope values, averaging −0.09/10a (per decade). The most pronounced drought trends are observed in the western regions, particularly in Huoerguosi City and Chabuchaer County, with slope values reaching −0.15/10a ($p < 0.05$). In contrast, the drought trend at the central Yining County station is relatively mild, with a slope of −0.03/10a. Overall, on an annual scale, the Ili River Valley exhibits an increasing drought trend, with the western regions experiencing a more significant drought trend compared to the relatively milder trends in the central and eastern regions.

3.3. Seasonal Variations in the SPEI in the Ili River Valley

Figure 5 illustrates the seasonal variations in the SPEI for the Ili River Valley, along with the results of the Mann–Kendall (M-K) test. The winter season is the only exception, exhibiting a wetting trend with SPEI values of 0.2/10a. In contrast, the other seasons show a significant trend toward increasing drought conditions, with the summer season displaying the most pronounced drought trend, with an SPEI of −0.16/10a.

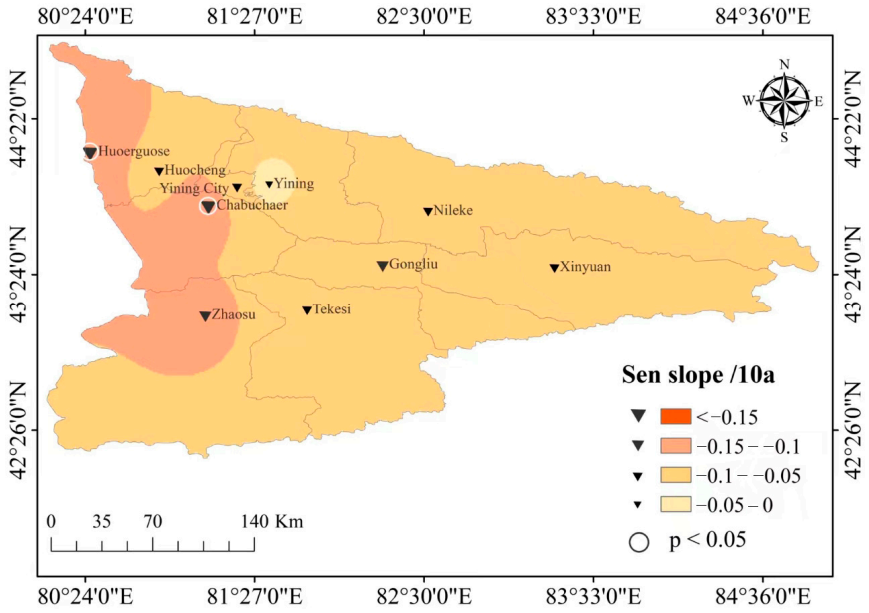


Figure 4. Temporal variations in SPEI in the Ili River Valley Region from 1961 to 2023.

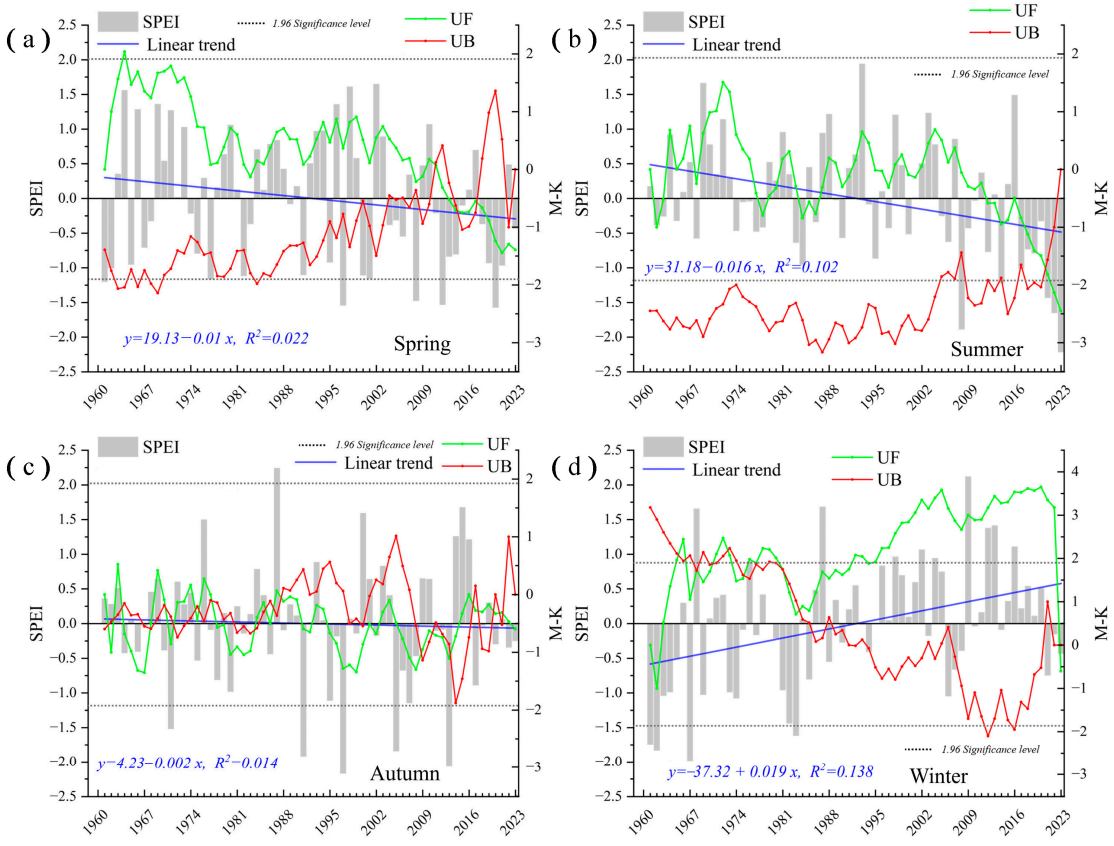


Figure 5. Changing characteristics of meteorological drought in the Ili River Valley from 1961 to 2023; spring (**a**), summer (**b**), autumn (**c**), and winter (**d**).

During the spring season (Figure 5a), the SPEI shows a downward trend, with values ranging from −1.57 to 1.65. The spring of 2002 was the most humid on record, while 2020 was the driest in the past 63 years. The SPEI time series from 1961 to 2003 reveals an initial rise followed by a decline, suggesting an overall drying tendency in spring for the region. The Mann–Kendall (M-K) test observed no significant shift in spring SPEI values.

In the summer (Figure 5b), the SPEI index follows a downward trajectory, with values ranging from −2.21 to 1.94. The summer of 1993 was the most humid on record, and 2023 was the driest. The SPEI time series from 1961 to 2007 showed an upward trend, followed by a marked drying trend. A distinct drought-related shift occurred in 2021 ($Z = -2.44$, $p < 0.01$), with an average annual SPEI reduction of 1.50.

Autumn shows a reduction in the SPEI (Figure 5c), with values ranging from −2.17 to 2.24. The autumn of 1987 was the wettest on record, while 1997 was the driest. The SPEI time series from 1961 to 1990 reflects an initial rise followed by a decline, indicating a general drying trend in autumn. No abrupt changes in the SPEI were noted.

For winter (Figure 5d), the SPEI index increases, with values ranging from −1.98 to 2.12. The winter of 1968 was the driest on record, while 2010 was the wettest. The SPEI index from 1961 to 1986 showed an initial decline followed by a significant increase, suggesting a wetter climate for the region. A notable shift in the SPEI occurred in 1984 ($Z = 3.17$, $p < 0.01$), with an average increase of 0.48.

In summary, the Ili River Valley exhibits a non-significant drying trend in both spring and autumn, a significant drying trend in summer, and a significant wetting trend in winter.

Figure 6 illustrates significant seasonal differences in the anomalies and cumulative anomalies of the SPEI in the Ili River Valley from 1961 to 2023. The SPEI changes in spring and summer generally follow interannual variations, while autumn and winter exhibit more notable differences.

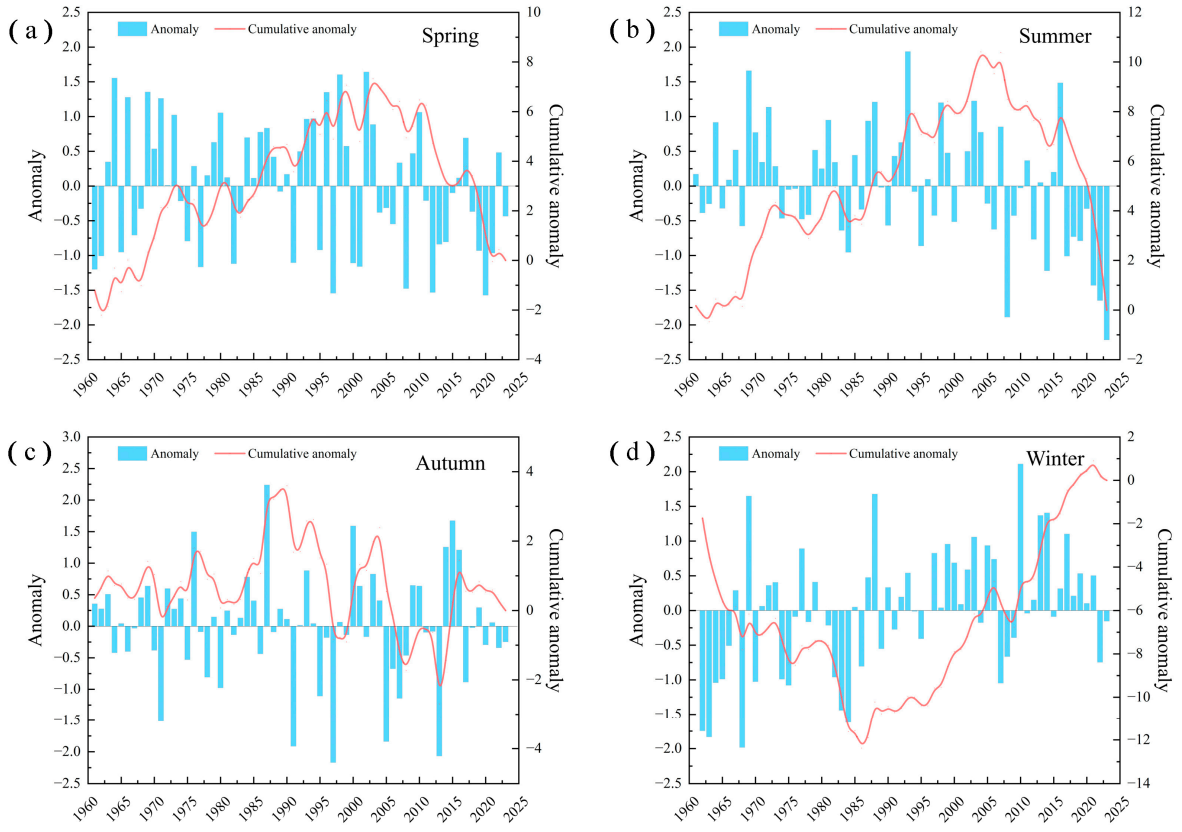


Figure 6. Variation trends in seasonal SPEI interannual anomalies and cumulative anomalies in the Ili River Valley from 1961 to 2023; spring (**a**), summer (**b**), autumn (**c**), and winter (**d**).

In spring and summer (Figure 6a,b), SPEI anomalies were predominantly positive between 1961 and 2004, indicating wetter periods. In contrast, from 2005 to 2023, the anomalies were mostly negative, suggesting drier periods. Additionally, the cumulative SPEI anomalies in spring and summer first increased and then decreased, forming an "inverted V" shape. Specifically, the cumulative SPEI anomaly in spring peaked at 7.32 in

2003, indicating a wet period before 2003 and a transition to drier conditions thereafter. Similarly, in 2004, the cumulative SPEI anomaly in summer reached its peak of 10.41.

Autumn exhibited more complex SPEI variations (Figure 6c). The period from 1961 to 1990 had more wet years, while from 1991 to 2023, there was an increase in years with negative anomalies, pointing to a trend toward aridification. The cumulative SPEI anomaly in autumn peaked at 3.60, in 1990.

Winter showed an inverse trend compared to the interannual changes (Figure 6d). From 1961 to 1986, the region experienced a drier period, while from 1987 to 2023, it transitioned into a wetter period. The cumulative SPEI anomaly in winter displayed a "V" shape, reaching its lowest value of −12.38 in 1986, signaling a drier period before 1986 and a subsequent shift toward wetter conditions.

As shown in Figure 7, there are significant spatial differences in the changes in the SPEI across different seasons in the Ili River Valley. The drought trends in spring, summer, and autumn generally align with the annual trends, all indicating a deepening of drought conditions. However, in winter, the Ili River Valley exhibits a notable wetting trend.

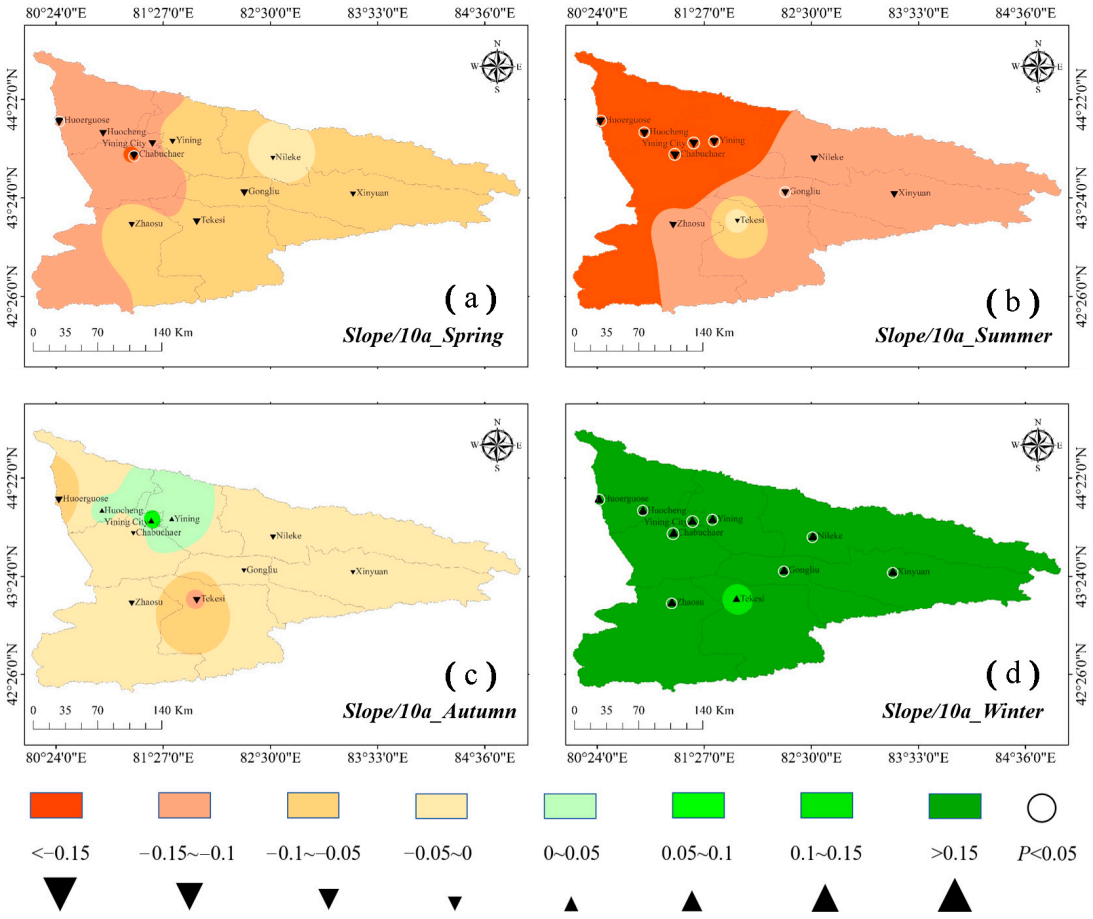


Figure 7. Spatial variation trends in seasonal SPEI in the Ili River Valley from 1961 to 2023; spring (**a**), summer (**b**), autumn (**c**), and winter (**d**).

From 1961 to 2023, the SPEI values in spring show a decreasing trend, with an average regional trend rate of −0.1/10a (Figure 7a). This trend is particularly pronounced and statistically significant ($p < 0.05$) at the stations in Huocheng City and Chabuchaer County. In summer (Figure 7b), the region overall displays a significant drought trend, with an average trend rate of −0.15/10a. The western part of the valley, including western Zhaosu and Gongliu counties, shows the most pronounced drought trend, while Tekesi County experiences a relatively mild trend. The autumn drought trend is somewhat alleviated

compared to spring and summer, with an average trend rate of −0.03/10a and no significant changes observed at any station (Figure 7c). The SPEI values at four stations, including Yining City and its surrounding counties (Yining, Huocheng, and Chabuchaer), exhibit an increasing trend, indicating a wetting pattern, while other stations, particularly Tekesi, show a drought trend.

In contrast to other seasons, winter demonstrates a significant wetting trend, with SPEI values increasing at all stations (Figure 7d). Nine stations, excluding Tekesi, pass the significance test, with an average regional trend rate of 0.2/10a.

3.4. Periodical Characteristics of the SPEI in Ili River Valley

Using wavelet periodic analysis, this study investigated the periodicity of the SPEI in the Ili River Valley from 1961 to 2023. As shown in Figure 8a,b, the results indicate significant drought variability on interannual time scales. The wavelet analysis identified two distinct drought variability cycles in the study area. The first is a long-term cycle with a period of 23 years, characterized by four alternating dry and wet phases over an average drought period of 15 years, persisting throughout the entire time series. The second is a shorter-term cycle with a period of 9 years, displaying approximately 10 alternating dry and wet phases over an average drought period of 6 years.

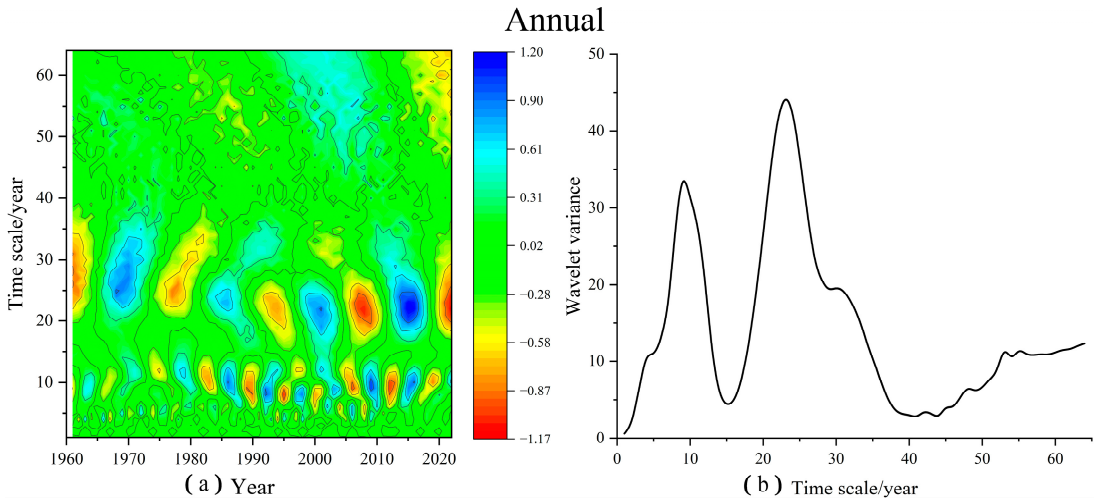


Figure 8. (**a**) Real contour map of the annual SPEI wavelet coefficients, (**b**) wavelet variance of the annual SPEI in the Ili River Valley from 1961 to 2023.

At the seasonal scale (as illustrated in Figure 9), distinct drought variability cycles are observed across different seasons. In spring (Figure 9(a1,b1)), significant periodic oscillations are detected on an 11-year timescale, with an average drought variability period of 7 years, during which eight dry–wet alternations occur. Additionally, a weaker periodic oscillation is observed on a 26-year timescale, with an average period of 17 years, encompassing approximately two dry–wet alternations. In summer (Figure 9(a2,b2)), significant periodic oscillations appear on a 21-year timescale, with an average drought variability period of 13 years and three dry–wet alternations. A weaker yet more frequent oscillation was recorded on an 8-year timescale, with an average period of 6 years, indicating relatively frequent dry–wet alternations. The drought variability cycle characteristics in autumn are similar to those in summer, with no significant differences in the main cycle, average period, or number of dry–wet alternations (Figure 9(a3,b3)). In winter, significant periodic oscillations are observed on a 31-year timescale, with an average drought variability period of 20 years, characterized by around two prominent dry–wet alternations (Figure 9(a4,b4)). Weaker periodic oscillations are also noted on a 17-year timescale, with an average period

of 11 years, including approximately five dry–wet alternations. Notably, in addition to the more prominent first and second principal cycles, drought variability across seasons is accompanied by some less pronounced small-scale periodic oscillations.

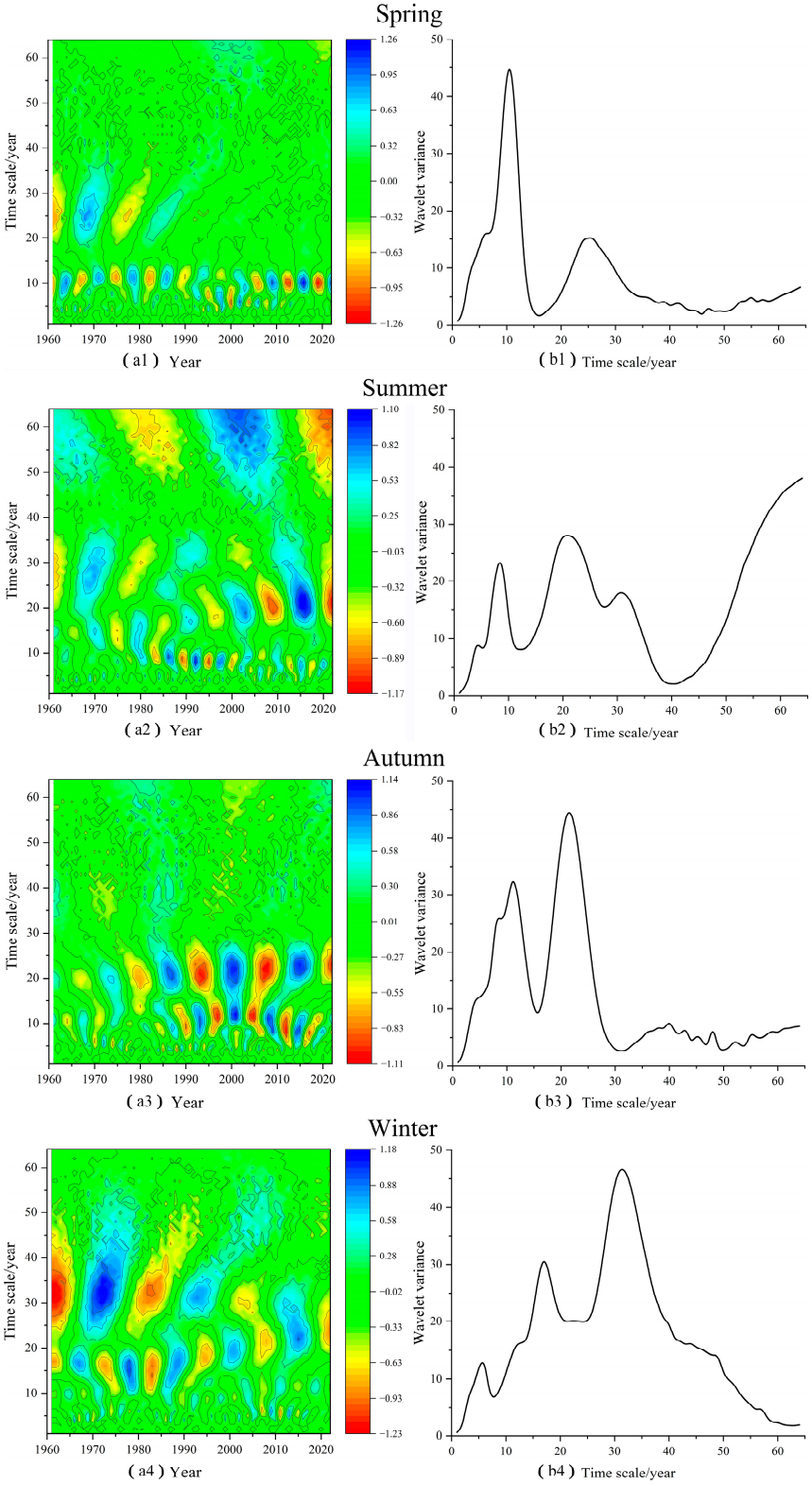


Figure 9. (**a1**–**a4**) Real contour map of the seasonal SPEI wavelet coefficients, (**b1**–**b4**) wavelet variance of the seasonal SPEI in the Ili River Valley from 1961 to 2023; spring (**a1**,**b1**), summer (**a2**,**b2**), autumn (**a3**,**b3**), and winter (**a4**,**b4**).

From the perspective of spatial variation (Figures 10 and 11), the characteristics of drought cycles across different locations within the Ili River Valley exhibit significant variability. On the interannual scale, the primary cycle timescales for Yining City and Zhaosu stations are 9 years and 14 years, respectively, with average periods of 6 years and 10 years. Other stations display primary cycle timescales ranging from 20 to 30 years, with corresponding average periods of 10 to 20 years. The secondary cycle timescales for Yining City and Zhaosu are 24 years and 15 years, respectively, while those for other stations are generally around 10 years, with average periods not exceeding 10 years.

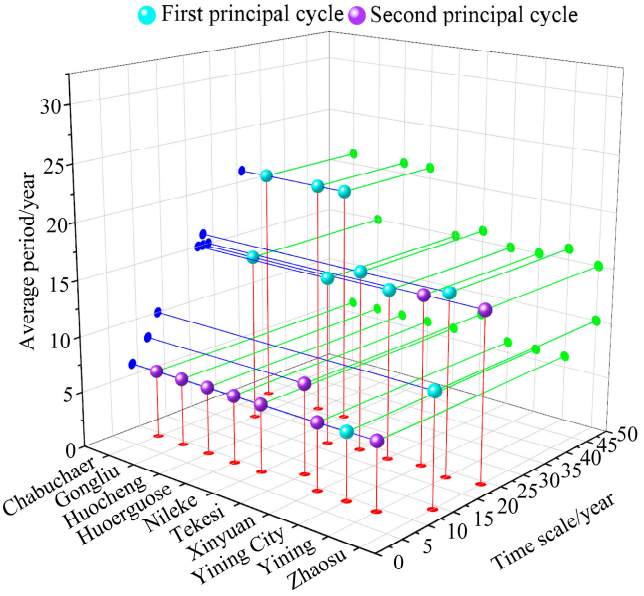


Figure 10. Three-dimensional scatter plot of the time scales and average periods of the SPEI on an annual scale at various stations in the Ili River Valley from 1961 to 2023.

At the seasonal scale, during spring (Figure 11a), Tekesi Station exhibits primary and secondary cycle timescales of 24a and 11a, with average periods of 16a and 8a, respectively. For the other stations, the primary cycle timescale is predominantly around 10a, with an average period of 7a, while the secondary cycle generally falls within 20–30a, with an average period of 10–20a. In summer (Figure 11b), Huocheng Station stands out with a long-period characteristic, displaying primary and secondary cycle timescales of 48a (average period of 30a) and 30a (average period of 19a), respectively. In contrast, Xinyuan and Zhaosu stations show relatively short primary cycles (9a timescale, 6a average period), with secondary cycles extending to 23a and 24a (average periods of 16a). For the remaining stations, the primary cycle timescale remains centered around 20–30a, with an average period of 10–20a, while the secondary cycle is approximately 8a with an average period of 5a. In autumn (Figure 11c), the primary cycles across stations can be categorized into two groups: those with approximately 20a and 10a timescales, corresponding to average drought periods of 5–15a. Winter presents more complex characteristics (Figure 11d), with stations such as Chabuchaer, Nileke, Tekesi, and Xinyuan showing primary cycle timescales ranging from 17 to 48a (average periods of 10–30a) and secondary cycle timescales ranging from 6 to 31a (average periods of 4–19a). The remaining stations demonstrate a primary cycle timescale of about 30a (average period of 20a) and a secondary cycle concentrated around 15a (average period of 10a).

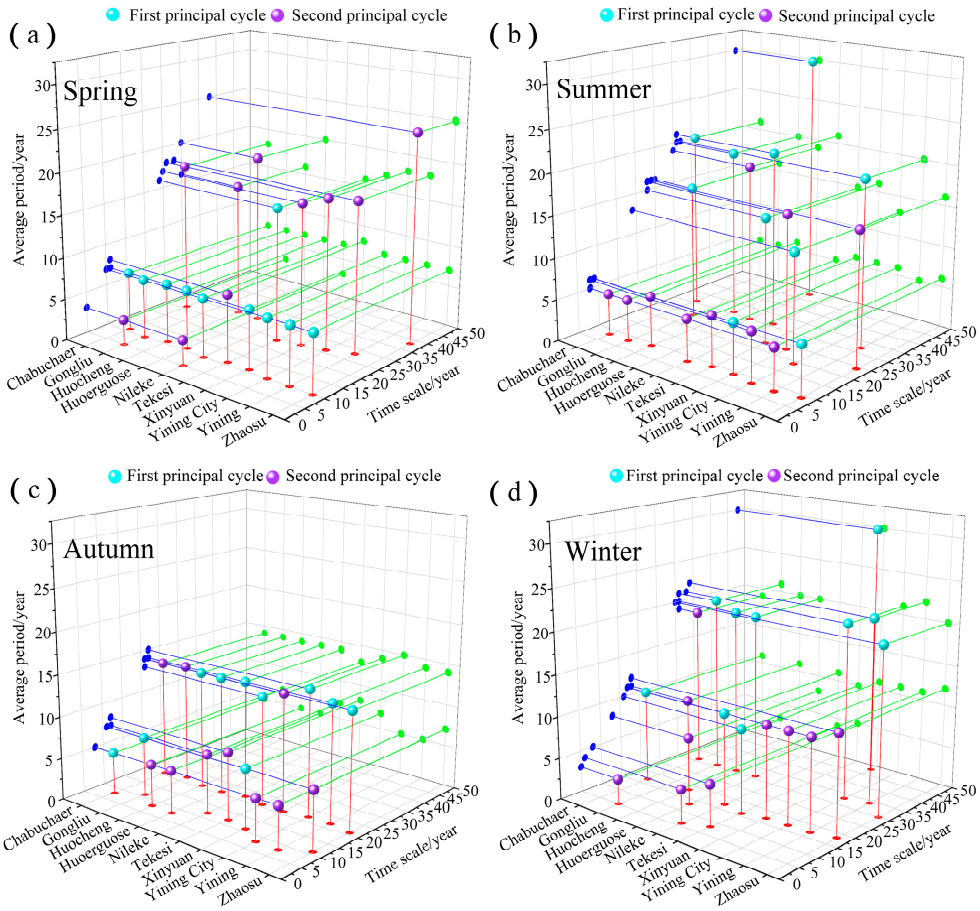


Figure 11. Three-dimensional scatter plot of the time scales and average periods of the SPEI on a seasonal scale at various stations in the Ili River Valley from 1961 to 2023; spring (**a**), summer (**b**), autumn (**c**), and winter (**d**).

4. Discussion

4.1. Drought Trends in Ili River Valley in Last 60 Years

Drought represents a significant environmental challenge in Xinjiang, China, an arid and semi-arid region. Since the 1990s, the region has experienced an increasing trend in drought, with a notable shift from a wetting to a drying trend around 1997 [42–44]. However, the drought dynamics in the Ili River Valley, a subregion of Xinjiang, appear to be distinct. Our analysis indicates that from 1961 to 2023 (Figures 2–4), drought severity in the Ili River Valley has shown a significant increasing trend since 1995, with no clear turning point between wet and dry periods. This trend does not entirely align with the broader drought patterns reported across Xinjiang [45]. Our findings suggest a divergent response, likely due to different time scales and regional variations within the broader Xinjiang region [21,43,46–48].

Notably, the drought trend in the Ili River Valley is approximately 0.09/10a (Figure 3), based on linear regression, which is less intense than the 0.122/10a trend observed for the broader Xinjiang region [47]. This discrepancy suggests that the Ili River Valley may be experiencing a milder drought intensity compared to other parts of Xinjiang. The underlying driver of these regional differences appears to be the complex interplay between temperature and precipitation patterns. Over the past two decades, significant increases in temperature without corresponding increases in precipitation have exacerbated the severity of meteorological drought in Xinjiang [43]. Climate model projections (CMIP6) further indicate that the region is likely to experience continued drying trends in the coming decades (2021–2100), with varying intensities ranging from −0.1/10a to −0.2/10a under

different emission scenarios [49]. However, whether the Ili River Valley will continue to exhibit a synchronized response to these broader aridification trends in Xinjiang remains an important topic for further investigation and discussion.

4.2. Seasonal Variations in Drought in the Ili River Valley

The analysis reveals pronounced seasonal variability in drought patterns within the Ili River Valley. A drying trend is observed during spring, summer, and autumn, while winter displays a tendency towards wetter conditions (Figure 4). This pattern aligns with findings from numerous studies in the broader Xinjiang region, though with varying intensities [21,50,51]. Specifically, in Xinjiang, the linear trend of the SPEI indicates a downward trajectory in spring, summer, and autumn, with k (slope) values above 0.11/10a, while the winter SPEI shows an upward trend with a k of 0.08/10a [52]. However, in the Ili River Valley, the SPEI in autumn shows more subtle changes, with k values of 0.02/10a, and the intensity of the spring drought (0.1/10a) is milder than the regional average for Xinjiang (0.13/10a). Notably, the Valley exhibits a significant trend towards aridification in summer, with a trend of 0.16/10a, higher than the aridification trend observed in Xinjiang (0.11/10a), characterized by an increasing frequency and severity of summer droughts [21,50]. This could be attributed to the weak increase in precipitation during significant warming periods in the region [43], or possibly the influence of altitude, as suggested by Zhang et al. (2021) [51]. In contrast to the summer, the Valley demonstrates a pronounced trend towards wetter conditions in winter, with a trend of 0.19/10a, significantly higher than the regional average in Xinjiang. This finding is consistent with the work of Jin et al. (2024), who reported a 17.3% increase in annual average precipitation in the Tianshan Mountains over the past 60 years, with a particularly striking 135.7% increase in winter precipitation [52].

The Mann–Kendall (MK) mutation analysis (Figure 4) further reveals that the Ili River Valley is experiencing abrupt changes in the dry seasons (spring, summer, autumn) several years later than the broader Xinjiang region [40,42], exhibiting a lagging response. For example, the Ili River Valley showed a 21-year lag for summer SPEI compared to the regional trends. In spring and autumn, delays of more than 17 and 35 years were observed, with no significant abrupt changes detected during these seasons in the Valley. This lagging response is also evident at the annual scale, where the Ili River Valley demonstrated a >25-year lag compared to the broader Xinjiang region, with no significant abrupt changes detected [45,46]. These findings suggest that the Ili River Valley exhibits greater resilience and resistance to the impacts of climate change, potentially due to factors such as its unique geographic characteristics or local climate dynamics, which may buffer the effects observed in the surrounding areas.

4.3. Spatial Variations in Drought Patterns Within the Ili River Valley

The spatial variability in meteorological drought within the Ili River Valley is further elucidated by analyzing the Sen's slope of the SPEI at various meteorological stations. The results indicate a more pronounced trend in aridification in the western Ili River Valley compared to the eastern part of the region. This disparity may be attributed to the distinct geographical characteristics of the two areas, with the western Ili River Valley comprising an oasis plain, while the eastern part is predominantly mountainous. This finding aligns with the conclusions of Zhang et al. (2021), who reported that the warming and wetting trends in the Tianshan region are primarily concentrated in ecological zones above 2800 m, while the densely populated low-lying oases are experiencing warming and drought [51]. In contrast, the Tekesi area in the central Ili River Valley exhibits a lower trend of aridification during the summer compared to the surrounding regions, but a higher trend in aridification in the autumn. The specific reasons for these divergent drought patterns in Tekesi County

relative to its neighboring areas warrant further detailed analysis, considering the unique topographical characteristics of the Tekesi region.

The observed spatial heterogeneity in drought trends within the Ili River Valley highlights the need for a nuanced understanding of the regional climate dynamics at play. The disparities between the western oasis plain, eastern mountainous regions, and the central Tekesi area underscore the importance of considering local-scale factors, such as terrain, land cover, and microclimatic conditions, when assessing the regional meteorological drought patterns.

4.4. Drought Periodicity in the Ili River Valley

This study also conducted a wavelet analysis of drought variability cycles at multiple temporal scales for both the entire Ili River Valley and ten monitoring stations located within each county and city. The results indicate that the Ili River Valley exhibits significant periodicity and dry–wet variation characteristics across various temporal scales, consistent with the overall drought variability patterns observed in the arid regions of northwestern China [21,53–55]. However, the dominant periodic scales of drought variation in the Ili River Valley (9-year and 15-year cycles) are longer than the average periodic scales observed in Xinjiang (5–8 years) [56]. This discrepancy suggests that the regional climate dynamics and drought patterns in this area are distinct and potentially more resilient to the impacts of climate change compared to the broader Xinjiang region. At the regional scale, the monitoring stations within the Ili River Valley demonstrate significant variability in drought cycle characteristics across different temporal scales and seasonal contexts. This finding highlights the complexity and heterogeneity of drought dynamics in the region, underscoring the importance of accounting for the influence of large-scale averages on localized, small-scale phenomena in future research.

The observed differences in drought periodicity between the Ili River Valley and the broader Xinjiang region suggest that local-scale factors play a crucial role in shaping the temporal patterns of drought variability. The longer periodic cycles detected in the Ili River Valley may reflect the unique climatic, hydrological, vegetal, and topographical features of this subregion, which can dampen the influence of large-scale drought drivers. Incorporating this spatial and temporal variability into drought monitoring and forecasting efforts will be essential for developing effective, targeted strategies to address the impacts of drought in the Ili River Valley.

5. Conclusions

This study identifies a significant increase in drought severity in the Ili River Valley since 1995, with no substantial shift from wetter to drier conditions. Seasonal analysis reveals considerable variability, with drying trends prevailing in spring, summer, and autumn, while winter conditions have become wetter. Although the annual and seasonal drought patterns in the valley generally align with broader trends observed in Xinjiang, they are characterized by milder intensity, particularly in spring and autumn. Spatially, the western oasis plain experiences more intense aridification compared to the eastern mountainous areas, underscoring the influence of local topography and land cover on drought dynamics. The delayed, abrupt changes in drought patterns within the valley further emphasize its relative resilience, suggesting that local climate dynamics and geographic characteristics play critical roles in moderating the impacts of broader climatic trends. Additionally, the valley demonstrates longer periodic drought cycles (9 and 15 years) compared to the regional average, indicating a distinct climatic response that may buffer against rapid climate fluctuations.

These findings underscore the need for region-specific drought monitoring to account for both temporal and spatial heterogeneities. Future research should aim to further investigate the underlying mechanisms driving these regional differences to enhance drought resilience in the Ili River Valley.

Author Contributions: Conceptualization, B.I. and A.A.; data curation, S.H.; writing—original draft preparation, S.H.; writing—review and editing, S.H. and B.I.; visualization, N.K. and Z.Z.; project administration and funding acquisition, B.I. All authors have read and agreed to the published version of the manuscript.

Funding: This study was supported by the National Natural Science Foundation of China (grant no. 32460279) and the Tianchi Fund Project of the Xinjiang Uyghur Autonomous Region, China (grant no. 2023TCYCQNBS01).

Data Availability Statement: The data presented in this study are available on request from the corresponding author.

Acknowledgments: The authors would like to thank Qingdong Shi from Xinjiang University for his contribution to this research. We have obtained his consent regarding this acknowledgment. We also appreciate the valuable comments and feedback provided by the reviewers and editors, which were instrumental in enhancing the quality of this work.

Conflicts of Interest: The authors declare no conflicts of interest.

References

1. Yuan, X.; Wang, Y.M.; Ji, P.; Wu, P.L.; Sheffield, J.; Otkin, J.A. A global transition to flash droughts under climate change. *Science* **2023**, *380*, 187–191. [CrossRef] [PubMed]
2. Zhang, J.; Wang, F. Changes in the risk of extreme climate events over East Asia at different global warming levels. *Water* **2019**, *11*, 2535. [CrossRef]
3. Yan, Z.; Ding, Y.; Zhai, P.; Song, L.; Cao, L.; Li, Z. Re-assessing climatic warming in China since 1900. *J. Meteorol. Res.* **2020**, *34*, 243–251. [CrossRef]
4. Wang, Y.; Ma, J.; Zhang, L.; Huang, Y.; Guo, X.; Yang, Y.; Zhao, E.; Zhao, Y.; Chu, Y.; Jiang, M. Spatial Distribution of, and Variations in, Cold Regions in China from 1961 to 2019. *Sustainability* **2022**, *14*, 465. [CrossRef]
5. Li, W.; Pan, R.; Jiang, Z.; Chen, Y.; Li, L.; Luo, J.J.; Zhai, P.; Shen, Y.; Yu, J. Future changes in the frequency of extreme droughts over China based on two large ensemble simulations. *J. Clim.* **2021**, *34*, 6023–6035. [CrossRef]
6. Cunha, A.; Zeri, M.; Leal, K.; Costa, L.; Cuartas, L.; Marengo, J.; Tomasella, J.; Vieira, R.; Barbosa, A.; Cunningham, C. Extreme drought events over Brazil from 2011 to 2019. *Atmosphere* **2019**, *10*, 642. [CrossRef]
7. Wan, L.; Bento, V.A.; Qu, Y.; Qiu, J.; Song, H.; Zhang, R.; Wu, X.; Xu, F.; Lu, J.; Wang, Q. Drought characteristics and dominant factors across China: Insights from high-resolution daily SPEI dataset between 1979 and 2018. *Sci. Total Environ.* **2023**, *901*, 166362. [CrossRef] [PubMed]
8. Li, P.; Omani, N.; Chaubey, I.; Wei, X. Evaluation of drought implications on ecosystem services: Freshwater provisioning and food provisioning in the Upper Mississippi River Basin. *Int. J. Environ. Res. Public Health* **2017**, *14*, 496. [CrossRef] [PubMed]
9. Xu, C.; Ke, Y.; Zhou, W.; Luo, W.; Ma, W.; Song, L.; Smith, M.D.; Hoover, D.L.; Wilcox, K.R.; Fu, W. Resistance and resilience of a semi-arid grassland to multi-year extreme drought. *Ecol. Indic.* **2021**, *131*, 108139. [CrossRef]
10. Jones, E.; van Vliet, M.T. Drought impacts on river salinity in the southern US: Implications for water scarcity. *Sci. Total Environ.* **2018**, *644*, 844–853. [CrossRef] [PubMed]
11. Zhang, D.; Zhang, Q.; Qiu, J.; Bai, P.; Liang, K.; Li, X. Intensification of hydrological drought due to human activity in the middle reaches of the Yangtze River, China. *Sci. Total Environ.* **2018**, *637*, 1432–1442. [CrossRef] [PubMed]
12. Cui, J.; Chen, A.; Huntingford, C.; Piao, S. Integrating ecosystem water demands into drought monitoring and assessment under climate change. *Nat. Water* **2024**, *2*, 215–218. [CrossRef]
13. Kim, W.; Iizumi, T.; Nishimori, M. Global patterns of crop production losses associated with droughts from 1983 to 2009. *J. Appl. Meteorol. Climatol.* **2019**, *58*, 1233–1244. [CrossRef]
14. Leng, G.; Hall, J. Crop yield sensitivity of global major agricultural countries to droughts and the projected changes in the future. *Sci. Total Environ.* **2019**, *654*, 811–821. [CrossRef] [PubMed]
15. Xu, C.; McDowell, N.G.; Fisher, R.A.; Wei, L.; Sevanto, S.; Christoffersen, B.O.; Weng, E.; Middleton, R.S. Increasing impacts of extreme droughts on vegetation productivity under climate change. *Nat. Clim. Chang.* **2019**, *9*, 948–953. [CrossRef]

16. Deng, Y.; Wang, X.; Wang, K.; Ciais, P.; Tang, S.; Jin, L.; Li, L.; Piao, S. Responses of vegetation greenness and carbon cycle to extreme droughts in China. *Agric. For. Meteorol.* **2021**, *298*, 108307. [CrossRef]
17. Piao, S.; Zhang, X.; Chen, A.; Liu, Q.; Lian, X.; Wang, X.; Peng, S.; Wu, X. The impacts of climate extremes on the terrestrial carbon cycle: A review. *Sci. China Earth Sci.* **2019**, *62*, 1551–1563. [CrossRef]
18. Song, L.L.; Tian, Q.; Li, Z.J. Response of Ecological Environment to Climate Change in the Source Area of the Yangtze River Based on the Observation During 2005-2015. *Pol. J. Environ. Stud.* **2021**, *12*, 13. [CrossRef]
19. Zhou, Q.; Huang, J.; Hu, Z.; Yin, G. Spatial-temporal changes to GRACE-derived terrestrial water storage in response to climate change in arid Northwest China. *Hydrol. Sci. J.* **2022**, *67*, 535–549. [CrossRef]
20. Pan, N.; Wang, S.; Liu, Y.; Li, Y.; Xue, F.; Wei, F.; Yu, H.; Fu, B. Rapid increase of potential evapotranspiration weakens the effect of precipitation on aridity in global drylands. *J. Arid Environ.* **2021**, *186*, 104414. [CrossRef]
21. Huang, W.; Yang, J.; Liu, Y.; Yu, E. Spatiotemporal variations of drought in the arid region of Northwestern China during 1950–2012. *Adv. Meteorol.* **2021**, *2021*, 6680067. [CrossRef]
22. Berg, A.; McColl, K.A. No projected global drylands expansion under greenhouse warming. *Nat. Clim. Chang.* **2021**, *11*, 331–337. [CrossRef]
23. Yan, X.; Cheng, P.; Zhang, Q.; Li, X.; He, J.; Yan, X.; Zhao, W.; Wang, L. Comparisons of climate change characteristics in typical arid regions of the Northern Hemisphere. *Front. Environ. Sci.* **2022**, *10*, 1033326. [CrossRef]
24. Daramola, M.T.; Xu, M. Recent changes in global dryland temperature and precipitation. *Int. J. Climatol.* **2022**, *42*, 1267–1282. [CrossRef]
25. Loh, P.S.; Mohammed Alnoor, H.I.; He, S. Impact of climate change on vegetation cover at south Port Sudan area. *Climate* **2020**, *8*, 114. [CrossRef]
26. Strydom, S.; Savage, M.; Clulow, A. Long-term trends and variability in the dryland microclimate of the Northern Cape Province, South Africa. *Theor. Appl. Climatol.* **2019**, *137*, 963–975. [CrossRef]
27. Li, L.; She, D.; Zheng, H.; Lin, P.; Yang, Z.L. Elucidating diverse drought characteristics from two meteorological drought indices (SPI and SPEI) in China. *J. Hydrometeorol.* **2020**, *21*, 1513–1530. [CrossRef]
28. Yao, N.; Li, L.; Feng, P.; Feng, H.; Li Liu, D.; Liu, Y.; Jiang, K.; Hu, X.; Li, Y. Projections of drought characteristics in China based on a standardized precipitation and evapotranspiration index and multiple GCMs. *Sci. Total Environ.* **2020**, *704*, 135245. [CrossRef] [PubMed]
29. Qi, Z.; Cui, C.; Jiang, Y.; Chen, Y.; Ju, J.; Guo, N. Changes in the spatial and temporal characteristics of China's arid region in the background of ENSO. *Sci. Rep.* **2022**, *12*, 17826. [CrossRef] [PubMed]
30. Chi, H.; Wu, Y.; Zheng, H.; Zhang, B.; Sun, Z.; Yan, J.; Ren, Y.; Guo, L. Spatial patterns of climate change and associated climate hazards in Northwest China. *Sci. Rep.* **2023**, *13*, 10418. [CrossRef] [PubMed]
31. Zhou, G.; Chen, Y.; Yao, J. Variations in precipitation and temperature in Xinjiang (Northwest China) and their connection to atmospheric circulation. *Front. Environ. Sci.* **2023**, *10*, 1082713. [CrossRef]
32. Liu, X.; Li, Y.; Ma, K.; Yang, L.; Li, M.; Li, C.; Wang, R.; Wang, N.; Deng, L.; He, M.-y. Spatial distribution and potential sources of arsenic and water-soluble ions in the snow at Ili River Valley, China. *Chemosphere* **2022**, *295*, 133845. [CrossRef] [PubMed]
33. Yang, H.; Sun, H.L.; Ye, M.; Ge, X.Y.; Wu, F.; Jin, X.L.; Wu, R. Characteristics of Vegetation Phenology Changes and Its Response to Climate Change in the Yili River Valley. *Acta Agrestia Sin.* **2024**, *32*, 859, (In Chinese with English Abstract). [CrossRef]
34. Shi, M.; Wu, H.; Fan, X.; Jia, H.; Dong, T.; He, P.; Baqa, M.F.; Jiang, P. Trade-offs and synergies of multiple ecosystem services for different land use scenarios in the yili river valley, China. *Sustainability* **2021**, *13*, 1577. [CrossRef]
35. Xu, Y.J.; Chen, Y.N.; Li, W.H.; Fu, A.H.; Ma, X.D.; Gui, D.W.; Chen, Y.P. Distribution pattern and environmental interpretation of plant species diversity in the mountainous region of Ili River Valley, Xinjiang, China. *Environ. Monit. Assess.* **2010**, *34*, 1142. [CrossRef]
36. Wang, Y.J.; Qin, D.H. Influence of climate change and human activity on water resources in arid region of Northwest China: An overview. *Adv. Clim. Chang. Res.* **2017**, *8*, 268–278. [CrossRef]
37. Li, L.; Li, J.; Yu, R. Characteristics of summer regional rainfall events over Ili River Valley in Northwest China. *Atmos. Res.* **2020**, *243*, 104996. [CrossRef]
38. Vicente-Serrano, S.M.; Beguería, S.; López-Moreno, J.I. A multiscalar drought index sensitive to global warming: The standardized precipitation evapotranspiration index. *J. Clim.* **2010**, *23*, 1696–1718. [CrossRef]
39. Allen, R.G.; Pereira, L.S.; Raes, D.; Smith, M. *Crop Evapotranspiration—Guidelines for Computing Crop Water Requirements*; FAO Irrigation and Drainage Paper 56; FAO: Rome, Italy, 1998; Volume 300, p. D05109.
40. Dakey, N.; Ren, J. Analysis of the spatial and temporal characteristics of drought evolution in Xinjiang from 1961 to 2020. *Water Sav. Irrig.* **2024**, *2*, 9–16, (In Chinese with English Abstract). [CrossRef]
41. Cohen, E.A.K.; Walden, A.T. A Statistical Study of Temporally Smoothed Wavelet Coherence. *IEEE Trans. Signal Process.* **2010**, *58*, 2964–2973. [CrossRef]

42. Yao, J.; Zhao, Y.; Chen, Y.; Yu, X.; Zhang, R. Multi-scale assessments of droughts: A case study in Xinjiang, China. *Sci. Total Environ.* **2018**, *630*, 444–452. [CrossRef] [PubMed]
43. Yao, J.; Zhao, Y.; Yu, X. Spatial-temporal variation and impacts of drought in Xinjiang (Northwest China) during 1961–2015. *PeerJ* **2018**, *6*, e4926. [CrossRef] [PubMed]
44. An, Q.; He, H.; Gao, J.; Nie, Q.; Cui, Y.; Wei, C.; Xie, X. Analysis of Temporal-Spatial Variation Characteristics of Drought: A Case Study from Xinjiang, China. *Water* **2020**, *12*, 741. [CrossRef]
45. Li, Q.; Chen, Y.; Shen, Y.; Li, X.; Xu, J. Spatial and temporal trends of climate change in Xinjiang, China. *J. Geog. Sci.* **2011**, *21*, 1007–1018. [CrossRef]
46. Hu, W.; Yao, J.; He, Q.; Chen, J. Changes in precipitation amounts and extremes across Xinjiang (northwest China) and their connection to climate indices. *PeerJ* **2021**, *9*, e10792. [CrossRef]
47. Yao, J.; Mao, W.; Chen, J.; Dilinuer, T. Recent signal and impact of wet-to-dry climatic shift in Xinjiang, China. *J. Geog. Sci.* **2021**, *31*, 1283–1298. [CrossRef]
48. Qu, L.-l.; Yao, J.-Q.; Zhao, Y. Mechanism analysis of the summer dry-wet interdecadal transition in the Tarim Basin, Northwest China. *Atmos. Res.* **2023**, *291*, 106840. [CrossRef]
49. Zhang, X.; Wang, X.; Zhou, B. CMIP6-projected changes in drought over Xinjiang, Northwest China. *Int. J. Climatol.* **2023**, *43*, 6560–6577. [CrossRef]
50. Li, M.; Yao, J.; Guan, J.; Zheng, J. Observed changes in vapor pressure deficit suggest a systematic drying of the atmosphere in Xinjiang of China. *Atmos. Res.* **2021**, *248*, 105199. [CrossRef]
51. Zhang, Y.; An, C.; Liu, L.; Zhang, Y.; Lu, C.; Zhang, W. High mountains becoming wetter while deserts getting drier in Xinjiang, China since the 1980s. *Land* **2021**, *10*, 1131. [CrossRef]
52. Jin, C.; Wang, B.; Cheng, T.F.; Dai, L.; Wang, T. How much we know about precipitation climatology over Tianshan Moun-tains—the Central Asian water tower. *npj Clim. Atmos. Sci.* **2024**, *7*, 21. [CrossRef]
53. Peng, Y.; Peng, T.; Li, Y. Spatiotemporal Characteristics of Drought in Northwest China Based on SPEI Analysis. *Atmosphere* **2023**, *14*, 1188. [CrossRef]
54. Zhang, Y.; Zhang, Y.; Cheng, L.; Cong, N.; Zheng, Z.; Huang, K.; Zhang, J.; Zhu, Y.; Gao, J.; Sun, Y. Have China's drylands become wetting in the past 50 years? *J. Geog. Sci.* **2023**, *33*, 99–120. [CrossRef]
55. Lian, L.; Liu, B. Change characteristics of dry and wet spells in northwest China during the past 58 years. *Arid Land Geog.* **2019**, *42*, 1301–1309. (In Chinese with English Abstract) [CrossRef]
56. Xuan, J.; Zheng, J.; Liu, Z. SPEI-based spatiotemporal variation of drought in Xinjiang. *Arid Zone Res.* **2016**, *33*, 338–344. (In Chinese with English Abstract) [CrossRef]

Disclaimer/Publisher's Note: The statements, opinions and data contained in all publications are solely those of the individual author(s) and contributor(s) and not of MDPI and/or the editor(s). MDPI and/or the editor(s) disclaim responsibility for any injury to people or property resulting from any ideas, methods, instructions or products referred to in the content.